Chemical and Process Engineering Research
ISSN 2224-7467 (Paper) ISSN 2225-0913 (Online)
Vol.39, 2015
www.iiste.org

Theoretically Investigation of the Heat Transfer Enhancement in a Horizontal Circular Tube

Ali hamzah Kadhim ALShabbani
University of Al-Qadissiya

Abstract
This work presents an experimental study to investigate the heat transfer enhancement in a horizontal circular tube use three metal oxide {(ZrO_2 (80nm), Al_2O_3(20nm), CuO (40nm))} distilled water nanofluids with twisted tape. Three types of twisted tapes (typical twisted tape, twisted tape with V-cut and clockwise- counter clockwise twisted tape) were used with twist ratios (TR=4, 6, 8). The studied concentrations of nanofluids are (φ=0, 0.01, 0.05, 0.1, 0.5, 1, 2, 3% by volume) under fully developed turbulent flow and uniform heat flux condition.
The numerical analysis was based on finite volume numerical techniques to solve the governing partial differential equations in three dimensions using ANSYS FLUENT commercial CFD software to study the effect of Reynolds number, concentration of nanofluid, concentration of nanofluid, nanofluid types and twist ratio on the heat transfer enhancement, average Nusselt number, velocity profile and skin friction for nanofluid. All the tests were carried out with Reynolds number range (2490-20100) and uniform heat flux (2108- 9280W/m^2).
Keywords: ANSYS FLUENT, Nanofluid, Heat Transfer, Circular Tube, Three metal oxide.

1. Introduction

In order to analyze the flow field in a tube with and without twisted tape under heat flux, a solution of continuity, Navier- Stokes equations as well as energy equation is required. Because of the complexity of twisted tapes configurations, it is possible to get an analytical solution of the governing equations for practical configuration. Numerical simulations allow the analysis of the complex geometry of the flow domain. Therefore, finite volume numerical techniques by ANSYS FLUENT code [1] have been used to solve those equations. The mixture of nanopartical and distilled water is assumed as a single phase to simplify the problem.

This research paper investigates the flow field in a tube with and without twisted tape and nanofluid using a governing partial differential equations in three dimensions which are based on conservation of mass, momentum and energy.

1.1 System geometry

The system geometry in the present work consists of a tube where the working fluid flows together with three types of inserts (typical twisted tape, twisted tape with V-cut, clockwise- counter clockwise twisted tape).
1.2. Tube geometry
The tube test section has a diameter and length (Din=0.01715m, Z=1.5 m), respectively. To ensure the flow is hydrodynamic fully developed, entrance length should be added to the test section length. For turbulent flow, the entrance length is according to the equation [2]

$$\frac{L_e}{D} = 4.4Re^{1/6} \quad (1)$$

Table (1): entrance length at different Reynolds numbers

Re	2490	4981	7472	9962	12700	14940	17440	19930
L_e (m)	0.277	0.311	0.333	0.350	0.364	0.374	0.384	0.392

And from table (1), it is noticed that the maximum length doesn't exceed (40 cm), so (50 cm) has been selected as entrance length for all the range of Reynolds number (1-A), the geometry is drawn using GAMBIT 2.4.6 software [3].

1.2 Twisted Tape Geometry

It is a metal strip of finite length twisted with different pitches and twist ratios (the pitch is a distance required for the strip to rotate 180°, and as shown in figure (1 B), the twist ratio is:

$$TR=\frac{P}{W} \quad (2)$$

The twisted tape is assumed in full contact with the internal surface of the tube, so the width of the tape is taken the same as the diameter of the tube (W=0.01715 m) and the tape length and thickness are (Z=1.5m, t=0.007 m).
The types of twisted tape used are (typical twisted tape, twisted tape with V-cut, clockwise- counter clockwise twisted tape). Three twist ratios (TR=4, 6, 8) are used in each type of twisted tape.
The dimensions of V-cut are taken from [6] who found the optimum cut depth ratio and width ratio as (DR=0.43, WR=0.34) respectively for all twist ratios as shown in figure (1C) where:

$$DR=\frac{e_d}{W} \quad (3)$$

$WR=\frac{e_w}{W}$ 4

The V-cut is located in each pitch in opposite direction to the previous one.

The clockwise-counter clockwise twisted tape changes its direction of rotation every two pitch distance (i.e., the tape rotate 360° in the clockwise direction along the distance "2P" and then it rotates in the counter clockwise direction 360° for the next distance "2P", this sequence will continue until the test section length reached, as shown in figure (2).

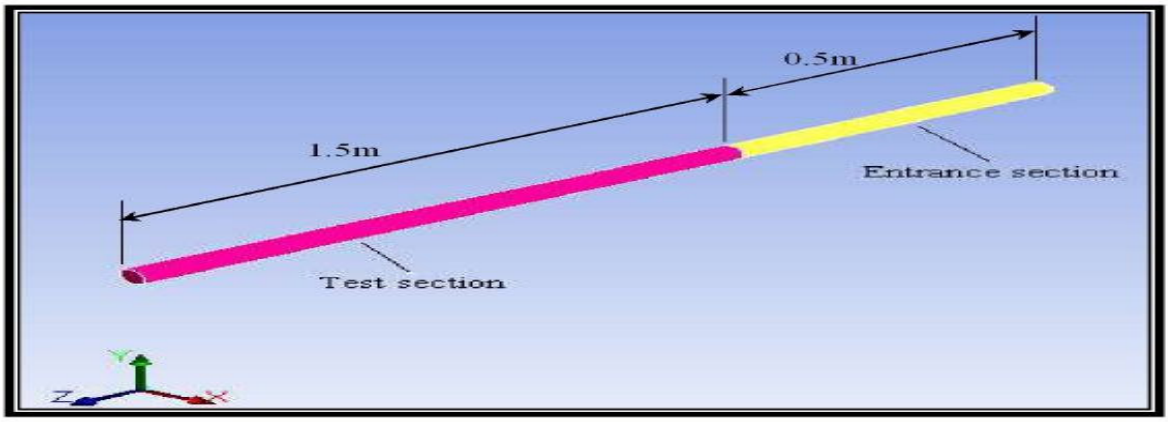

(A): Dimensions of typical twisted tape

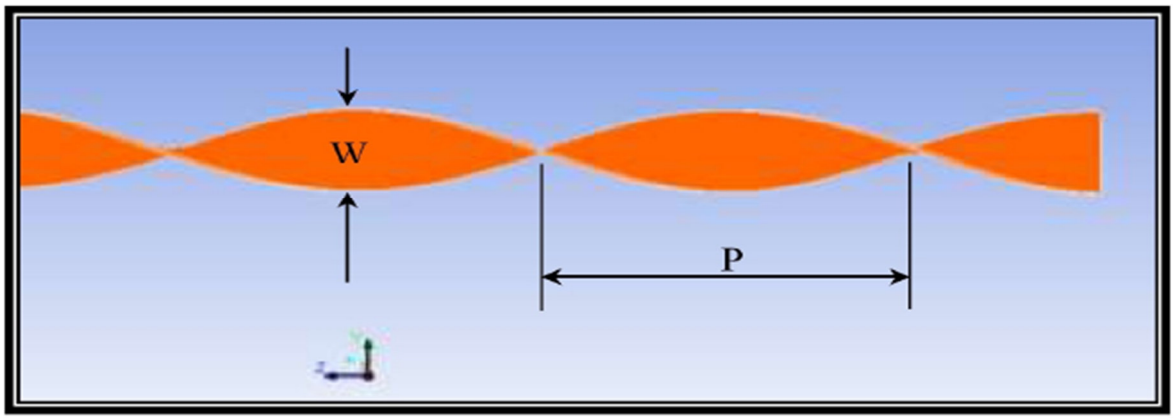

(B) Dimensions of typical twisted tape

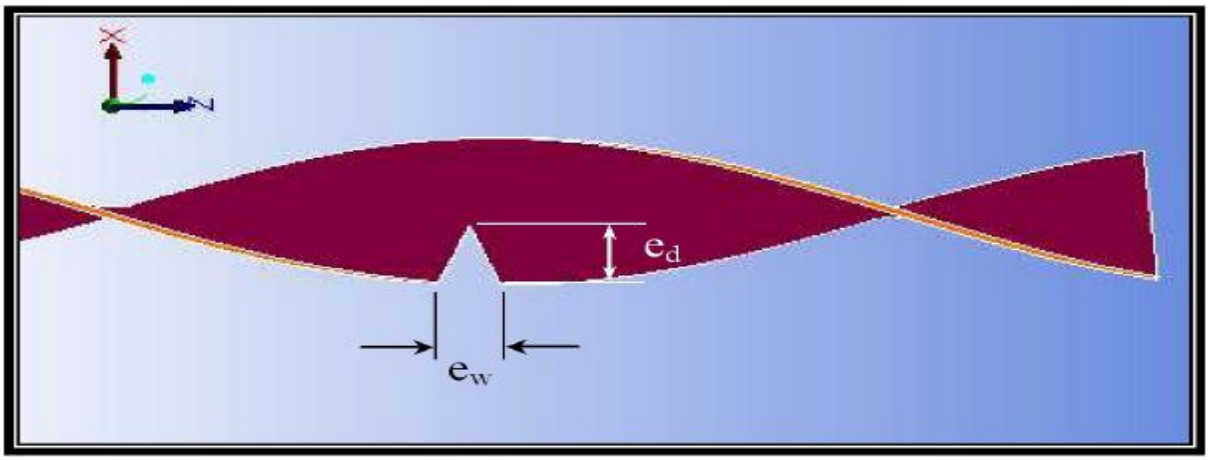

(C): Dimensions of V-cut twisted tape

Figure (1): Dimensions of different types of twisted tape

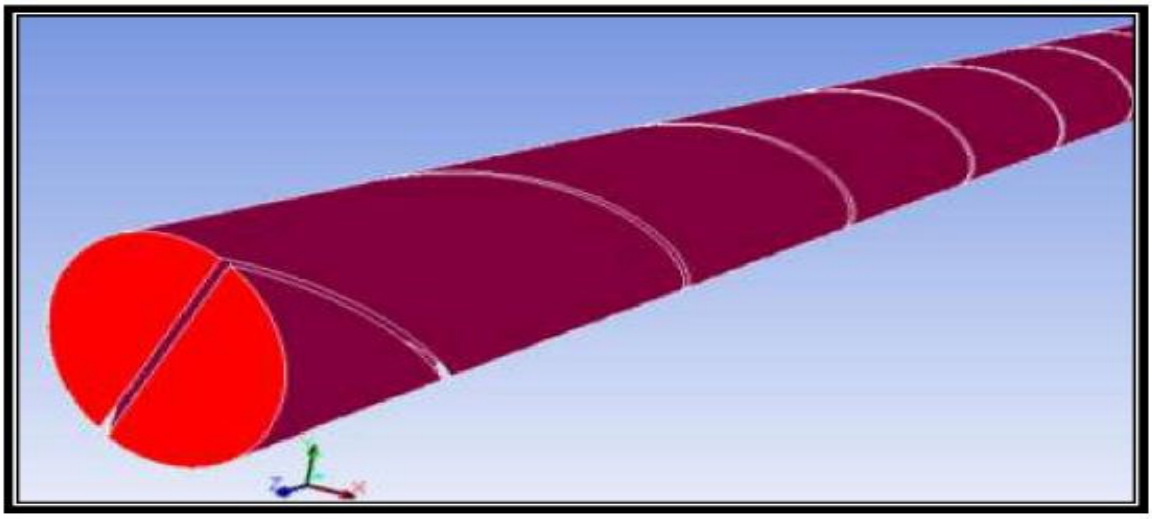

Figure (2): Shapes of different types of twisted tape

For the computational model, the geometry is generated by using GAMBIT 2.4.6 software to build the tube and the tapes and the tapes and the domain of fluid flowing between them as a three- solid dimensional, as shown in figure (3).

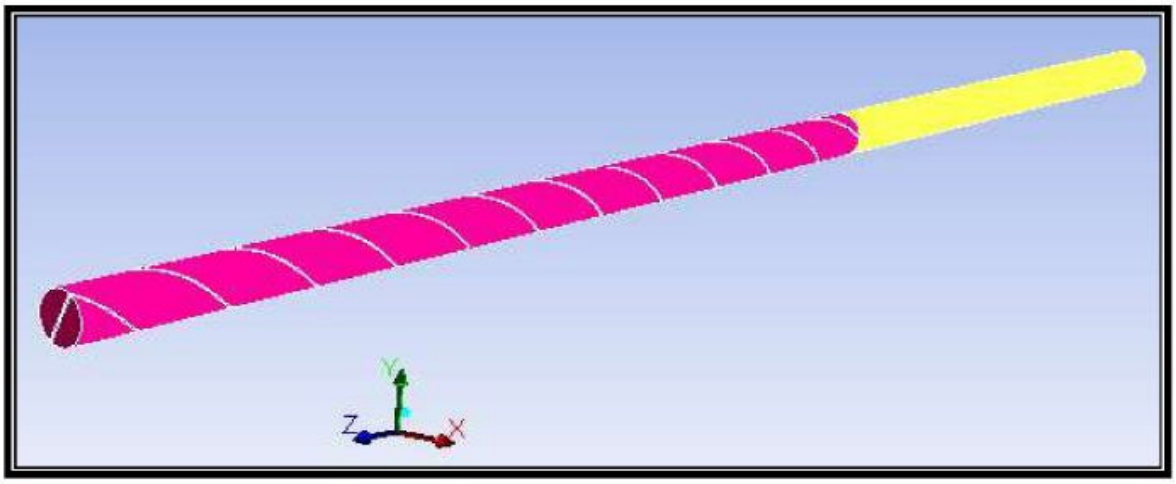

Figure (3): Three- dimensional solid model of fluid flowing between tube and the tapes

2. Basic Governing Equations:

The single phase conservation equations for continuity, momentum and energy equations and the turbulent model are used [4] under the following assumptions:

1) Steady atate
2) Incompressible fluid
3) Newtonian fluid
4) Turbulent flow
5) Three dimensional

4. Transport Equation of Turbulence

The distribution of eddy viscosity throughout the flow domain must be evaluated in order to calculate the momentum and heat diffusion coefficients for turbulent equations. This is the job of turbulent model.

The model used in the present work was Realizable k-ϵ (RKE) model [5] which provides superior performance for flows involving rotation, boundary layers under strong adverse pressure gradients, separation and recirculation, suitable for complex flows involving severe pressure gradient, separation, strong streamline curvature.

The transport equations for the Realizable k-ϵ model[5] in tensor form:

5. Physical properties of Nanofluids

The effective physical properties of the mixtures studied were measured for studied concentrations. These properties are viscosity, density and specific heat.

And for the difficulty of measuring the thermal conductivity, the property was calculated using empirical formula by Vajjha [6] which is formulated the three types of nanofluids used (ZrO2, Al2O3 and CuO- distilled water).

$$k_{nf} = \frac{k_p + 2k_{bf} - 2(k_{bf} - k_p)\varphi}{k_p + 2k_{bf} + (k_{bf} - k_p)\varphi} k_{bf} + 5\times10^4 \beta\varphi\rho_{bf} C_{bf} \sqrt{\frac{K\,T}{\rho_p\, d_p}}\, f(\varphi)$$

$$f(\varphi) = (2.821\times10^{-2}\,\varphi + 3.917) + (-3.0669\times10^{-2}\,\varphi - 3.91123\times10^{-3})$$

6. Mesh Generation

Standard CFD methods require a mesh that fits the boundaries of the computational domain. It is impractical to find a single general mesh generation technique that fits the whole range of problems. Therefore, it is rather preferred to employ a suitable technique that is best adapted to the considered type of engineering application.

The generation of mesh for a complex geometry is time consuming and often requires modifications to the model geometry. There are generally two types of approaches in volume meshing; structured and unstructured meshing. The structured mesh, however, is extremely inefficient and time consuming for complex geometries. Therefore, it has been excluded in this research as the geometry being considered complex and contains many details. In the unstructured approach, the grids are in general successful for complex geometries. However, the quality of these grids deteriorates with complex shapes. In addition, there is a large computational overhead owing to a large number of operations per node.

6.1 Polyhedral Mesh

In the present paper, the structural mesh will not be used and the unstructured mesh will be a possible alternative. There are many possibilities to generate unstructured meshes to be used in CFD analysis, the tetrahedral element may be used to generate unstructured mesh. However, this element may experience a high skewness, Figure (4), in the region of steep gradient in geometries and produces unsuccessful mesh quality for a complex geometry.

$$\text{Face skewness} = 1 - \frac{\textit{length of shorter face diagnol}}{\textit{length of longer face diagnol}} \qquad (13)$$

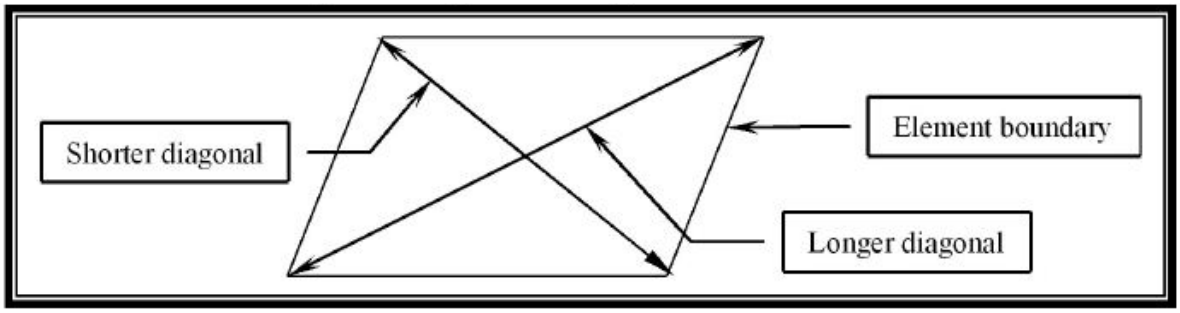

Figure (4): Skewness over all cell faces

For the present paper, a unique polyhedral mesh, figure (5 C) is used.

This mesh allows the flexibility of an unstructured mesh to be applied to a complex geometry without the overhead associated with a large tetrahedral mesh. This can reduce the overall cell count by a factor of 3 to 5 [7]. Alternatively, cell-skewness based agglomeration can be used to convert regions with highly skewed cells to a polyhedral, thereby improving mesh quality. The automatic nature these mesh agglomeration techniques saves the run time and since the polyhedral mesh contains as few as 1/5 the number of cells in the original tetrahedral mesh, convergence is faster. It should be noted that polyhedral mesh cannot be created directly from within the Gambit code since Gambit does not support for a three dimensional polyhedral mesh. The mesh is created into two types:

Step I: Three dimensional tetrahedral meshes are generated using Gambit code.

Step II: polyhedral meshes are created using automatic cell agglomeration within FLUENT code to convert tetrahedral cells into polyhedral ones. Figure (6) shows the tetrahedral Figure (6 A) and the polyhedral figure (6 C) meshes for the fluid in a tube with twisted tape model.

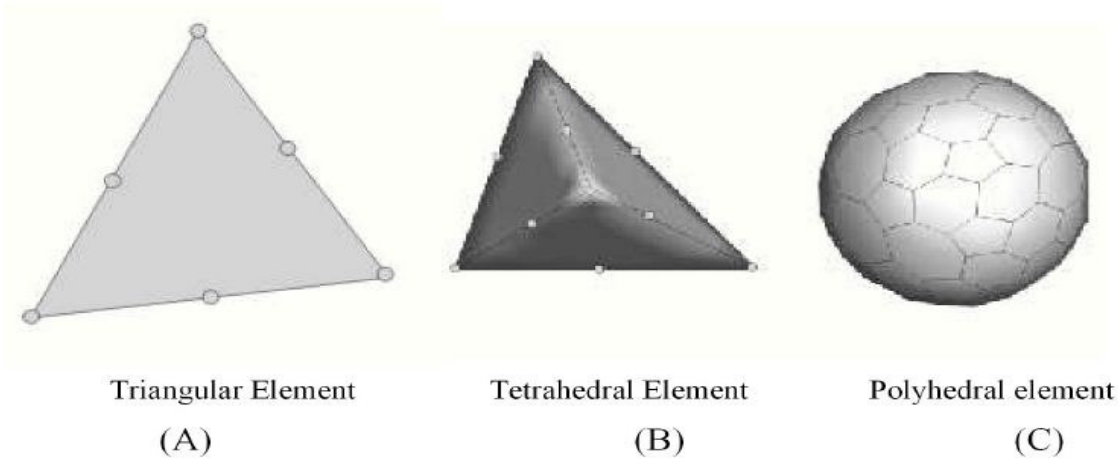

Figure (5): (A) triangular element type, (B) Tetrahedral element type and (C) Polyhedral element type

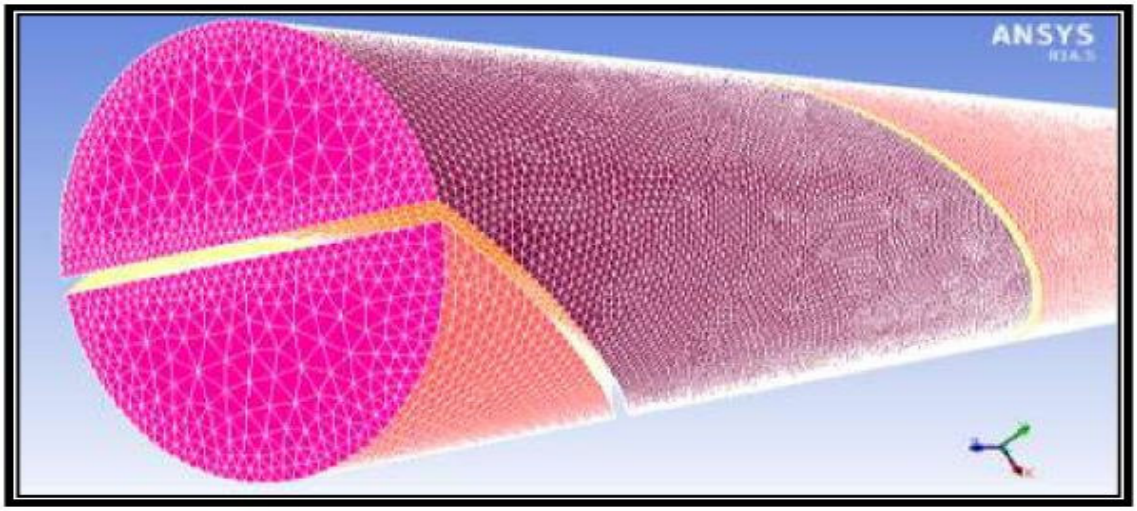

(A) Tetrahedral mesh created in Gambit code

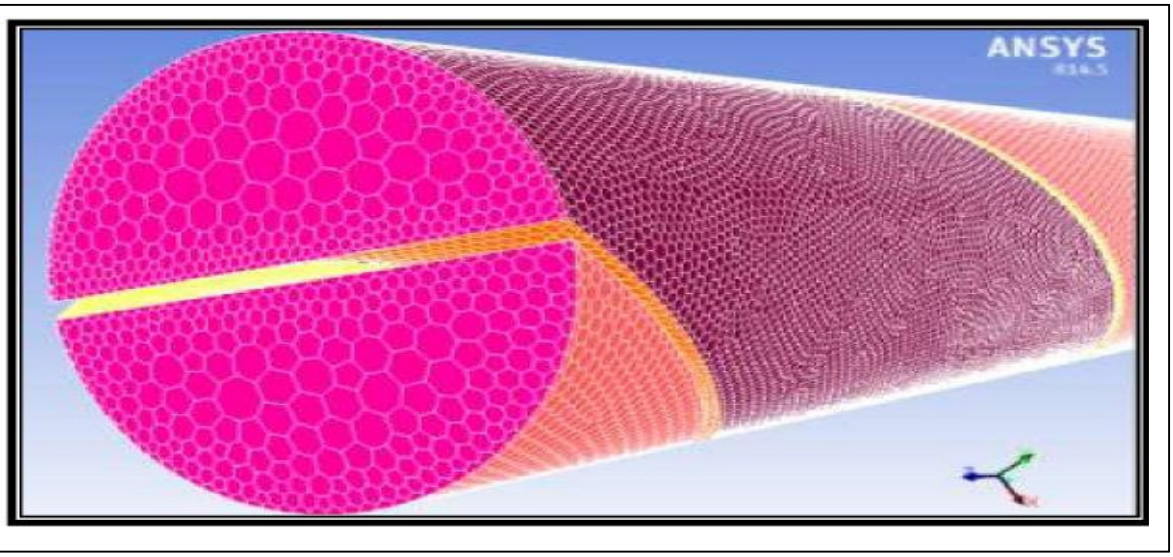

(B) Polyhedral mesh created in Fluent code
Figure (6): Mesh of the fluid domain in a tube with twisted tape

6.2 Three Dimensional Mesh Generation

It is more durable to divide the mesh generation process into subsequent steps including two major issues for further controlling of the mesh. This may have included the followings:

I. Surface mesh generation
II. Volume mesh generation

I. Surface mesh generation

Surface mesh is created for the geometry including the tube surface and twisted tape surface. A triangular element, figure (7) is used to generate a three-dimensional pave unstructured surface mesh.

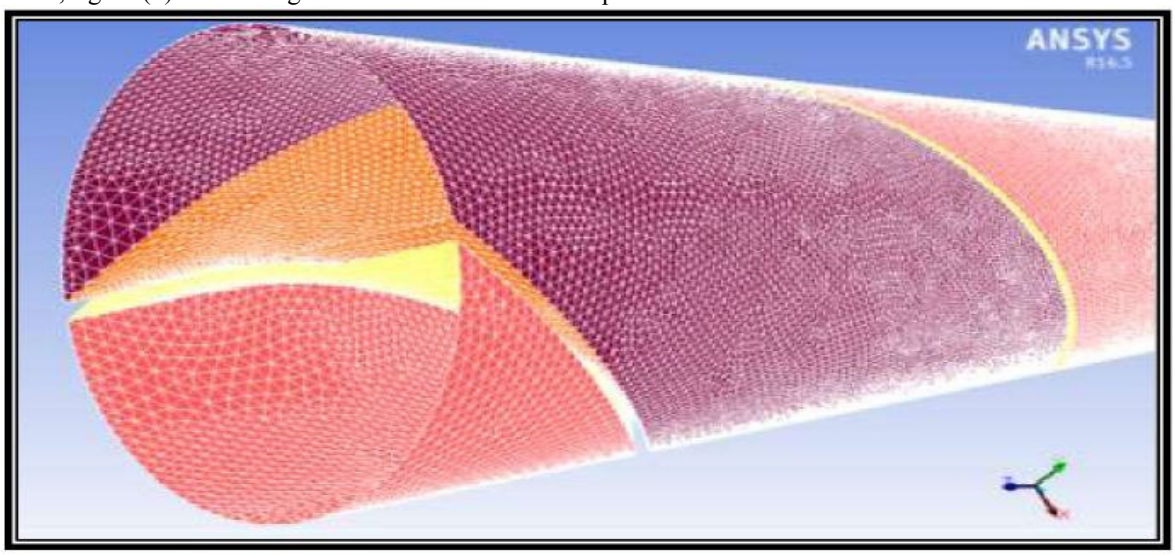

Figure (7) Triangular element mesh of the boundary surfaces

II. Volume mesh generation

When all surfaces were meshed for each individual area, the volume mesh can now be created for each zone (entrance section and test section) comprising a closed loop of area using T-Grid scheme. Building the mesh requires fine cells in area near tube and twisted tape surfaces so that it is convenient for turbulent flow characterized. On the other hand, using this element size in the whole domain would lead to an enormous number of elements. That is why it was decided to use a fine mesh in the region near to the surfaces and use coarse meshes as the distance from the surface grows.

Therefore, the mesh should be manipulated and controlled manually to keep smooth mesh transition and maintain accurate mesh for a three dimensional model with a minimum computational expense, this has been achieved through the following:

I. Applying boundary layer mesh
II. Applying size function

6.2.1 Boundary Layer Mesh

Boundary layer mesh defines the spacing of mesh node rows in regions immediately adjacent to surface area. They are used primarily to control mesh density and thereby to control the amount of information available from the computational model in specific regions of interest.

For the present work, the boundary layer mesh is attached to the tube and twisted tape surfaces as shown in figure (8). To define a boundary layer mesh, the following information must be specified (Table 2):

Table(2) summary of the characteristics of the boundary layer mesh used for computational domain

Zone				Algorithm	Number of rows	Growth factor	Attached Face
Test section (Twisted tape zone)	Uniform	8	1.2	Tube and twisted tape surfaces			

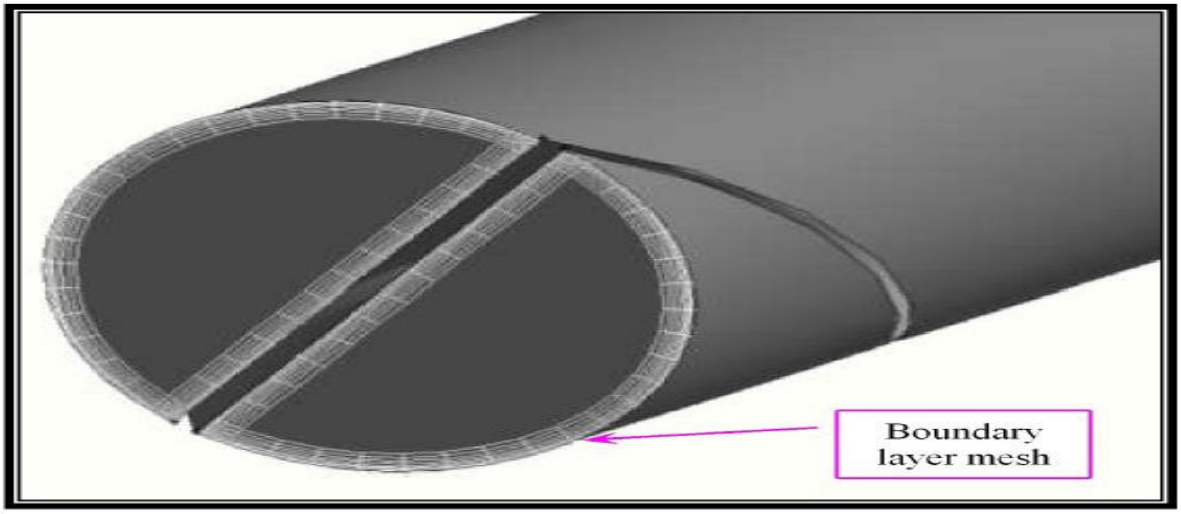

Figure (8) Boundary layer mesh of the boundary surfaces

6.2.2 Size function

Size functions are used to control the size of mesh intervals for edges and mesh elements for faces or volumes and thus to keep smooth transition of mesh from fine mesh near the tube surface to coarse mesh far away at the undisturbed boundaries as shown in figure (6). To create a size function**, the following specifications must be defined:**

- **Type**
- **Entities**
- **Parameters**

The type specification determines the algorithm used by the size function to control the mesh-element edge size. The entities specification determines the geometric entities that are used as the source and attachment entities for the size function. The size function parameters define the exact characteristics of the size function.

6.3 Mesh quality and Dependency

It is very important to assess this mesh for quality and dependency prior to run to ensure that accurate results can be successfully obtained.

There are some general guidelines to create a good mesh. A good mesh should be fine enough with high quality and good distribution. Moreover, the mesh should not have more cells than the available computer resources can handle. These guidelines are Quality, Resolution and Total cell count. Since similar boundary conditions and mesh strategy have been adopted for all models of twisted tape and nanofluid types, it is good to take the V-cut twist tape with TR=4 as the case study for quality and dependency check.

6.3.1 Mesh Quality

It is important to investigate mesh quality and check the elements orientation. The importance of quality parameter is the face alignment, it is the parameter that determines skewness of cells by equation (13). Elements with high skewness and severely distorted and it should be avoided to have such distorted cells in the critical regions. Highly skewed cells are not only adversely affect the accuracy but also they may lead to divergence. This value is about (0.2-0.4).

6.3.2 Mesh Resolution

A grid independent solution is the one for which a finer grid gives the same results with the original one and the results do not change as the grid gets finer. The way of checking whether the solution is grid independent or not is to create a grid with more cells to compare the solutions of the two models. Grid refinement tests for Nusselt number indicate that a grid size of approximately (4.1) million cells provide sufficient accuracy and resolution to be adopted as the standard for all cases.

The grid independency test performed for V-cut twist tape with TR=4 configuration is shown in figure (9).

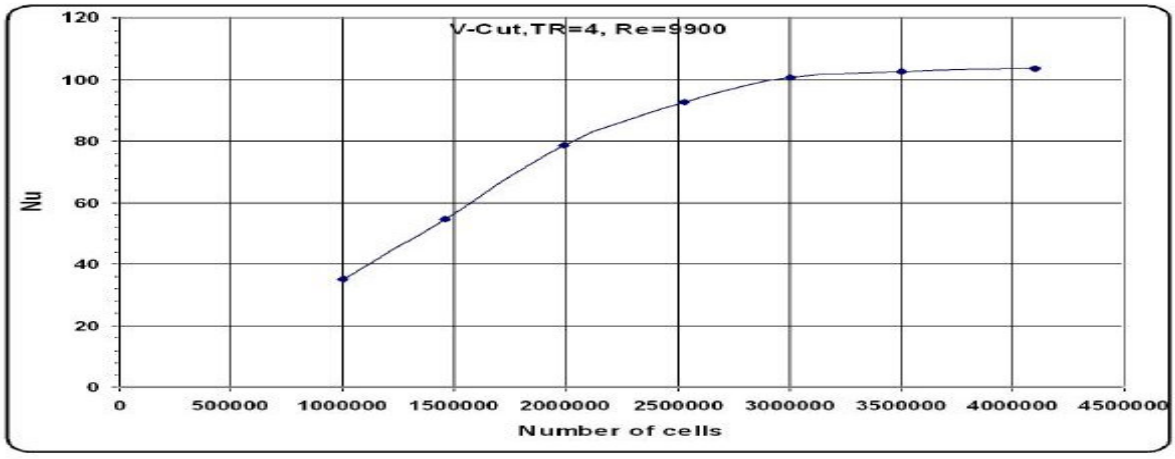

Figure (9) The grid independent solution test for V-cut twist tape with TR=4

6.3.3 Total cell count

The final point in a good mesh is the total number of cells generated. It is vital to have enough number of cells for a good resolution but the memory requirements increase as the number of cells increase.

7. Solution

A control-volume based technique that consists of the following steps is used for solution [8]:

1) A grid is generated on the domain.

2) for velocity, pressure and conserved scalars, algebraic set of equations and constructed by the integration of the governing equations on each control volume.

3) Discretized equations are linearized and solved iteratively.

7.1 Number of Iteration and Convergence Criteria

This is the maximum number of iterations done before the solver terminates. During the iterative process, the residuals were carefully monitored. For all simulations performed in the present paper, converged solutions were considered when the residuals resulting from the iterative process for all governing equations did not change with the iteration progress and the computational error may be ignored then the iteration manually stopped. For most of the cases, the iterations is around (2000-2500). Figure (10) shows the convergence history for continuity, momentum and energy equations. Average minimum convergences were (2×10^{-5}, 2×10^{-7} and 1×10^{-8}) for continuity, velocities and energy equations respectively for laminar flow cases and residuals of (2×10-7 and 4×10-7) for k and ε respectively.

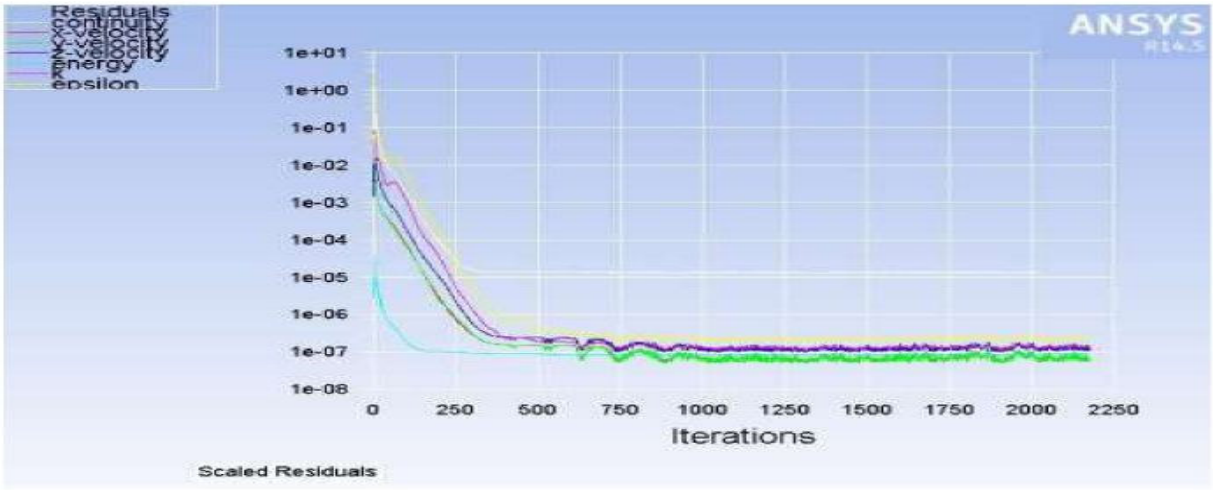

Figure (10) Convergence history for continuity, momentum, energy and turbulence equations

7.2 Discretization scheme

Finite volume method is used to convert the integral equations to algebraic forms. The pressure- velocity coupling is solved using SIMPLE algorithm with Second Order Upwind scheme for momentum, turbulence and energy equations for better accuracy. In the calculations, the standard pressure interpolation scheme is used. It is suitable for most kinds of problems.

Fluent solves the linear systems resulting from discretization schemes using a point implicit (Gauss- Seidel) linear equation solver in conjunction with an algebraic multigrid method.

8. Implementation of the boundary conditions

Boundary conditions are specified for each zone of the computational domain, Figure (10). However, the internal domain does not require any boundary conditions. It has been assigned as a fluid.

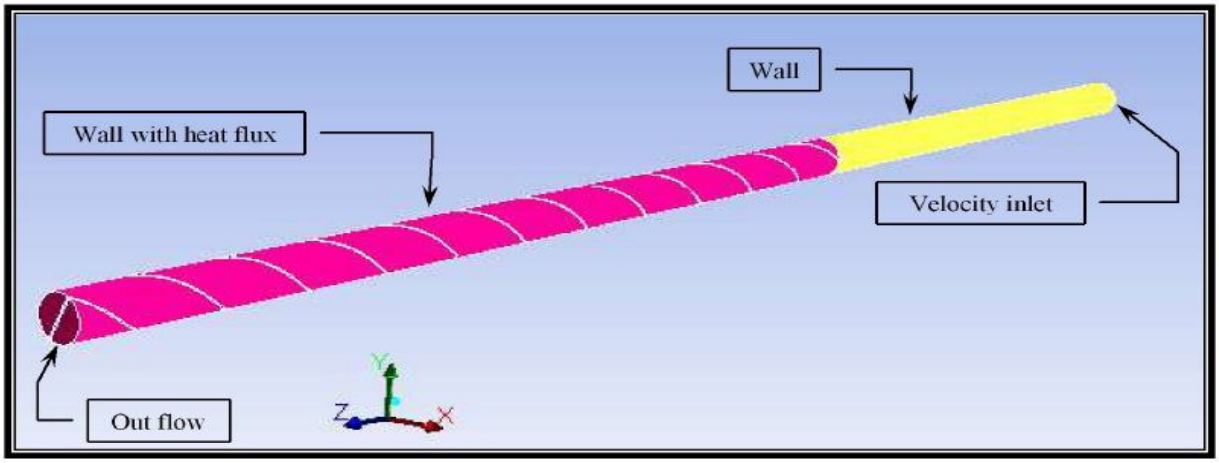

Figure (11) Boundary condition of the computational domain

8.1 Velocity Inlet Boundary Condition

The velocity inlet to the tube is specified over a range of (0.14-1.174 m/sec) depending on the flow rate of the working fluid.constant temperature inlet to the tube is 20℃.

Table (4) velocity values corresponding to flow rate values

Q(L/min)	2	4	6	8	10	12	14	16
W (m/s)	0.146	0.293	0.44	0.587	0.748	0.88	1.027	1.174

8.2 Wall Boundary Conditions

No slip boundary condition is specified for the twisted tape and tube surfaces and is set as a wall. the tube wall of the test section is subjected to a uniform heat flux in the range (2108- 9280 W/m^2).

8.3 Outlet Boundary Conditions

Out flow is specified at the outlet of the test section domain, where the total flow exits at this section.

9. Results and Discussion

Numerical results were carried out using the finite volume method single-phase model by commercial CFD program (FLUENT) and for all the specified conditions of (φ =0.01, 0.05, 0.1, 0.5, 1, 2, 3% by volume), (Re=2490-20100) and twist ratios (TR=4, 6, 8).

Figures (12),(13) and (14) show the Nusselt number for the three types of nanofluids (ZrO2,Al2O3 and CuO) in a plain tube respectively.

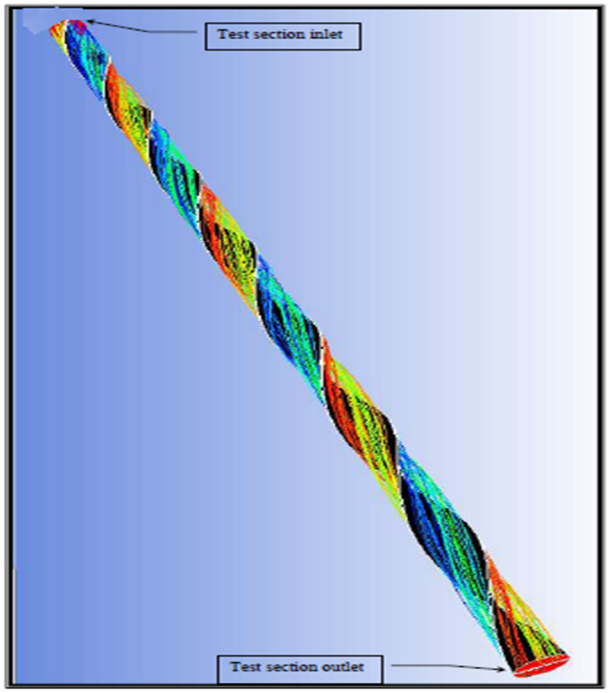

Figure (12) path lines of the flow in a tube fitted with typical twisted tape TR=4.

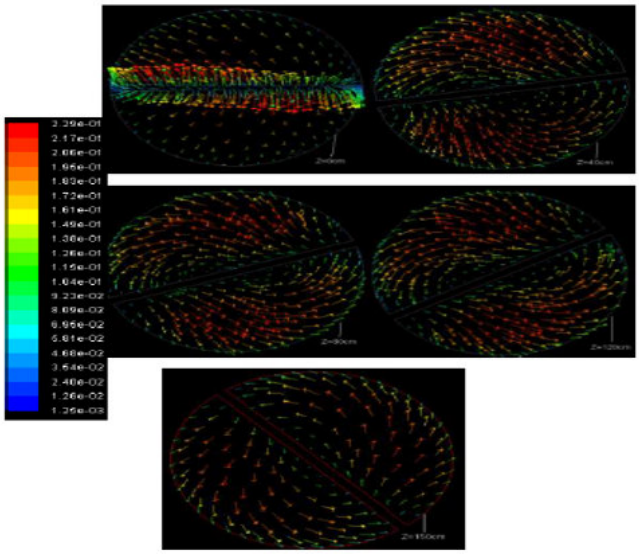

Figure (13) Velocity vector in (m/s) at locations of (Z=0, 40, 80, 120, 150 cm) along the test section for typical twisted tape with (Re=2490, TR=4).

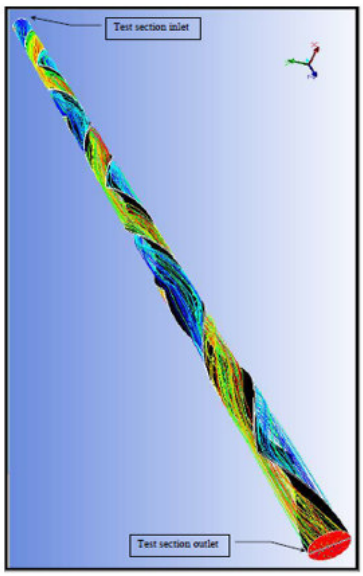

Figure (14) path lines of the flow in a tube fitted with V-cut twisted tape TR=4.

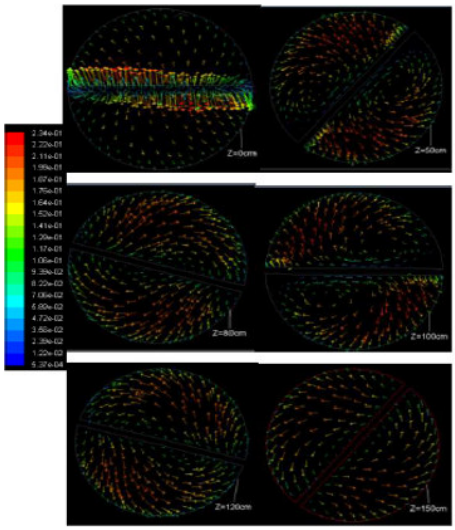

Figure (15) Velocity vector in (m/s) at locations of V-cuts along the twisted tape in test section for V-cut twisted tape with (Re=2490, TR=4).

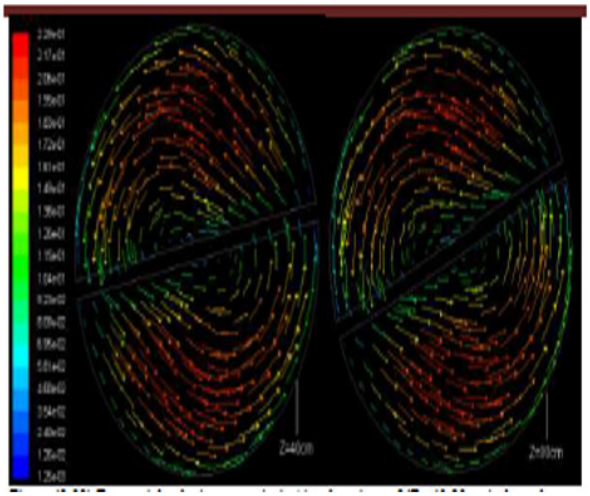

Figure (16) Tangential velocity vector in (m/s) at locations of (Z=40.80 cm) along the test section for typical twist tape with (Re=2490, TR=4).

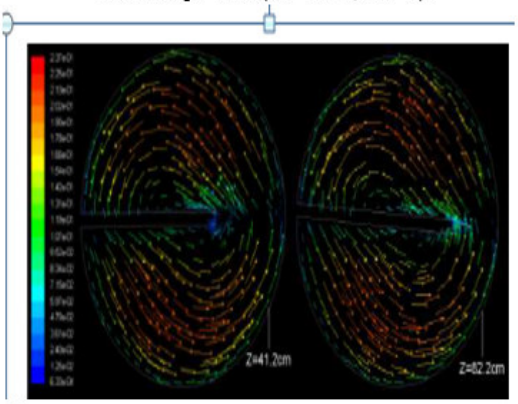

Figure (17) Tangential velocity vector in (m/s) at locations of V-cuts (Z=41.2, 61.7 cm) along the twisted tape in test section for V-cut twisted tape with (Re=2490, TR=4).

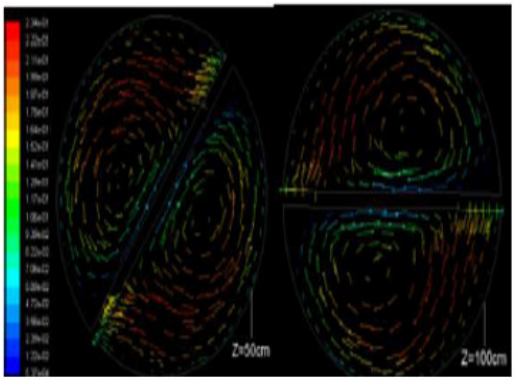

Figure (18) Tangential velocity vector in (m/s) at locations of V-cuts (Z=50, 100 cm) of converting from clockwise to counter clockwise along the test section for clockwise-counter clockwise twisted tape with (Re=2490, TR=4).

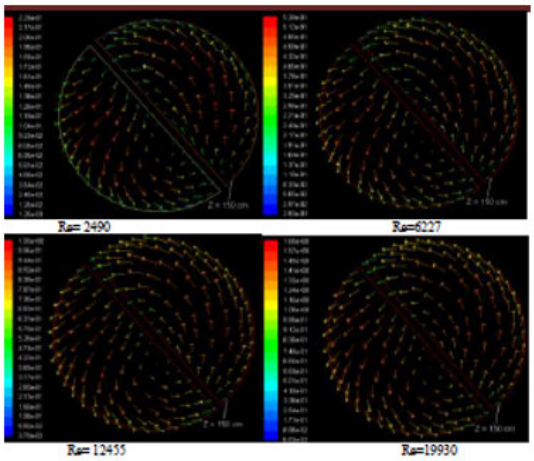

Figure (19) Velocity vector in (m/s) at the exit of the test section for typical twisted tape at TR=4 with the specified Reynolds numbers.

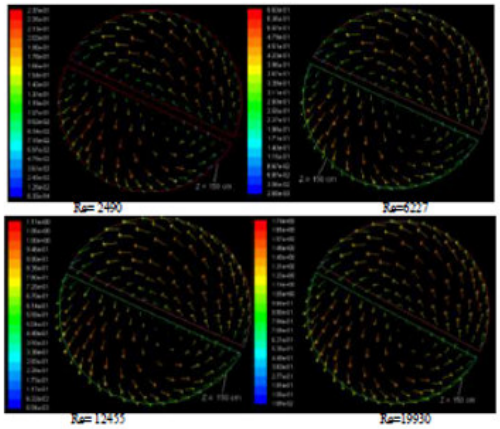

Figure (20) Velocity vector in (m/s) at the exit of the test section for V-cut twisted tape at TR=4 with the specified Reynolds numbers.

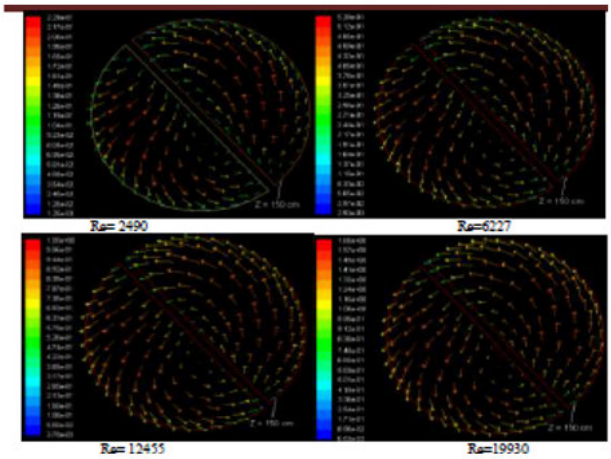

Figure (21) Velocity vector in (m/s) at the exit of the test section for clockwise-counter clockwise twisted tape at TR=4 with the specified Reynolds numbers.

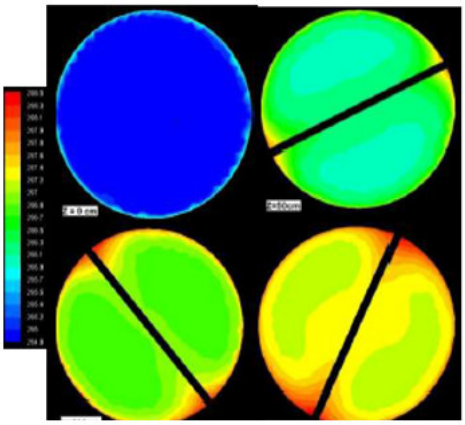

Figure (22) Temperature contours in (K) at locations of (Z=0, 50, 100, 150 cm) along the test section for typical twisted tape with (Re=2490).

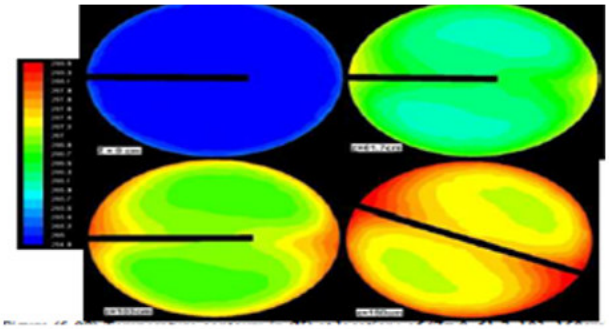

Figure (23) Temperature contours in (K) at locations of (Z=0, 61.7, 103,150 cm) along the test section for V-cut twisted tape with (Re=2490).

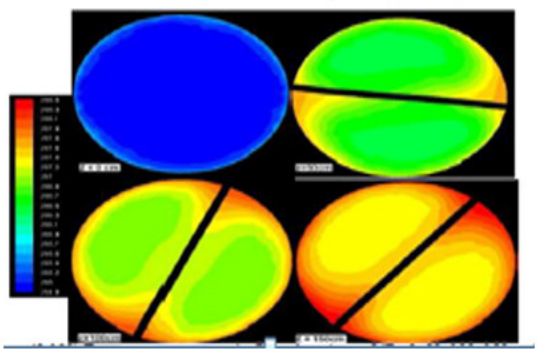

Figure (24) Temperature contours in (K) at locations of (Z=0, 50, 100,150 cm)along the test section for clockwise-counter clock wise twisted tape with (Re=2490).

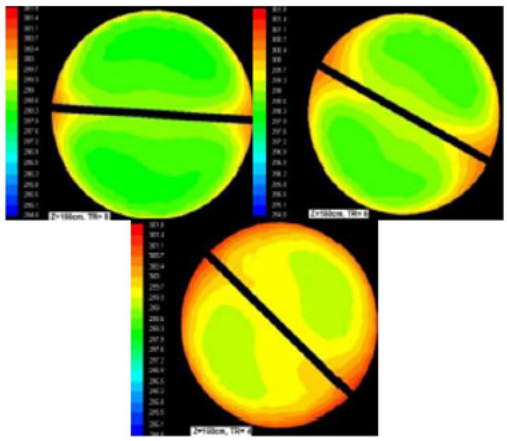

Figure (25) Temperature contours in (K) for the used twist ratios (4, 6, 8) at exit of the test section for (CuO, Re=6227,φ = 3%) and clockwise-counter clockwise twisted tape.

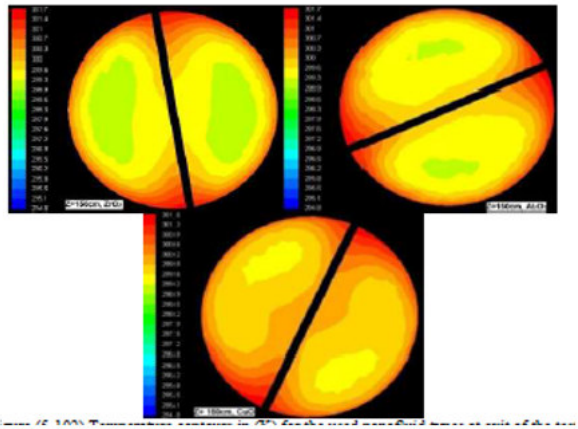

Figure (26) Temperature contours in (K) for the used nanofluid types at exit of the test section for the clockwise-counter clockwise twisted tape with (Re=2490, φ = 3%, TR=4).

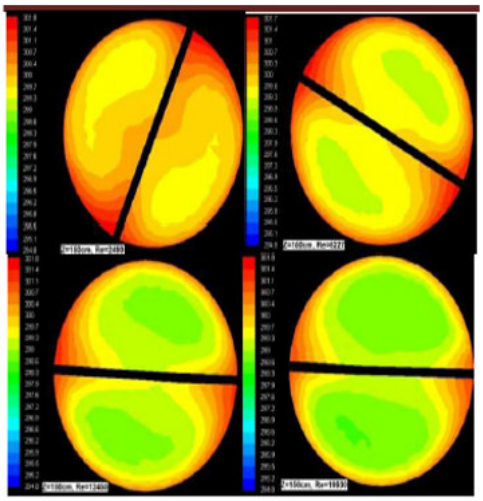

Figure (27) Temperature contours in (K) for different Reynolds number at exit of the test section for typical twisted tape (Al_2O_3, φ = 3%, TR=4).

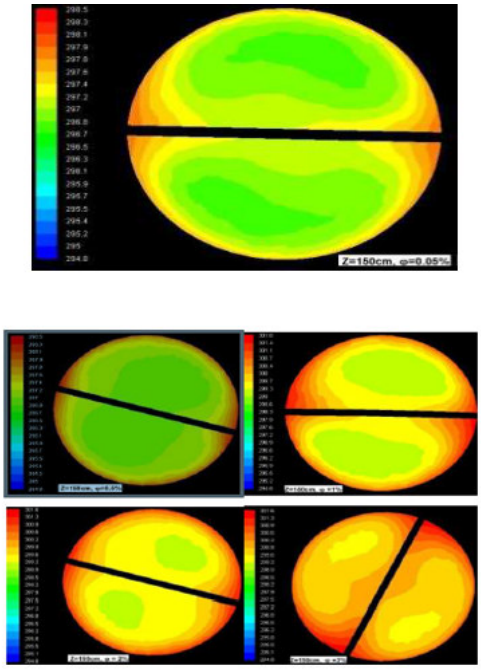

Figure (28) Temperature contours in (K) for different concentrations at exit of the test section for the clockwise-counter clockwise twisted tape with (Re=2490).

Conclusions

1. The nanofluid higher enhances the heat transfer compared with the base fluid (distilled water) in general with little increase of pressure drop. The nanofluid (CuO-distilled water) shows more heat transfer enhancement compared with γAl2O3-distilled water and ZrO2 distilled water. The heat transfer enhanced with increasing nanoparticles concentration and (φ=3%) gives higher heat transfer enhancement among the studied concentration.
2. The use of twisted tape also increases the heat transfer enhancement. The twist ratio (TR=4) gives higher Nusslet number compared to (TR=6,8) and the clockwise-counterclockwise type yields higher Nusslet number compared to the other types.
3. The individual use of twisted tape illustrates the maximum heat transfer enhancement (2.41 times Nusslet number of the plain tube) which occurs with twist ratio (TR=4).

4. The combined use of the nanofluid and twisted tape gives higher heat transfer enhancement compared to the individual use of each one. Also, this shows that the maximum enhancement in the heat transfer (7.5 times Nusslet number of the distilled water) and thermal performance factor was 3.9 for CuO with clockwise-counterclockwise twisted tape and twist ratio (TR=4) at Reynolds number 2490 and concentration (φ =3%).
5. The use of finite volume method single-phase model in ANSYS FLUENT commercial CFD software generally gives good agreement and it is suitable for predicting the pipe flow with both nanofluid and twisted tape.
6. The temperature of the flow increases and becomes more homogeneous with increasing flow rate, concentration and decrease with the twist ratio.

References

[1] ANSYS FLUENT, Version 14.5, ANSYS Inc. 2013.
[2] Frank M. White, "Fluid Mechanics", Fourth edition, Mac Graw-Hill books, 2001.
[3] Gambit, cortex version 2.4.6, Fluent Inc.,2004.
[4] ANSYS FLUENT, Version 14.5, ANSYS Inc.2013, "Fluent 14.5 User's Guide", 2013.
[5] Shih T., Liou W., Shabbir A., Yang Z. and Zhu J.," A New κ-ε Eddy-Viscosity Model for High Reynolds Number Turbulent Flows – Model Development and Validation". Computers Fluids. 24(3). 227–238. 1995.
[6] Fluent User Services Center, www.fluentusers.com
[7] Ravikanth S. Vajjha, Debendra K. Das, "Experimental determination of thermal conductivity of three nanofluids and development of new correlations", International Journal of Heat and Mass Transfer 52 (2009) 4675–4682.
[8] Patankar, S.V., "Numerical heat transfer and fluid flow", Hemisphere publishing corporation, Taylor & Francis group, New York, 1980.
[9] Versteeg, H. K., and Malalasekera, W., "An introduction to computational fluid dynamics-The finite volume method", Longman group Ltd., 1995.